Laser-excited site-selective spectroscopy of Eu^{3+} in sphene ($CaTiSiO_5$) and glasses and glass ceramics of the sodium-calcium-aluminum titanosilicate system

J. A. Capobianco,* T. F. Belliveau, G. Lord, and D. J. Simkin
Department of Chemistry, McGill University, Montreal, Quebec, Canada H3A 2K6

J. Tait and P. J. Hayward
Whiteshell Nuclear Research Establishment, Atomic Energy of Canada Limited, Pinawa, Manitoba, Canada R0E 1L0

(Received 18 March 1986)

The $^5D_0 \rightarrow {}^7F_0, {}^7F_1, {}^7F_2$ emissions of europium(III) in a glass (sodium aluminosilicate), sphene ceramic [calcium titanosilicate ($CaTiSiO_5$)], and glass ceramic (microcrystalline sphene in a sodium aluminosilicate glass matrix) are reported. Fluorescence-line-narrowed emission excited by the $^5D_0 \leftarrow {}^7F_0$ transition was used to sample the different coordination sites of Eu^{3+} represented by the inhomogeneously broadened absorption band. From the ratios of crystal-field parameters of the same order (B_{22}/B_{20} and B_{44}/B_{40}) obtained from fitting the observed energy levels assuming C_{2v} site symmetry, it was found that the sites Eu^{3+} occupies in the glass are adequately described by Brecher and Riseberg's model of a ninth coordinating oxygen atom approaching a distorted Archimedian antiprism of oxygen atoms along the C_2 axis. At least two different coordination sites exist in the sphene ceramic, neither of which fits the above coordination scheme, but at least the geometrical coordination appears constant. Emission from Eu^{3+} in both the glass and sphene phases was observed from the glass-ceramic samples. Furthermore, a Eu^{3+} partitioning ratio of 8:1 (sphene phase to glass phase) is estimated from the ratios of integrated emission intensities.

I. INTRODUCTION

Laser-excited site-selective spectroscopy, or fluorescence-line narrowing (FLN), is a useful technique for studying structural inhomogeneities in both crystals and glasses. Since it was first applied to ruby by Szabo,[1] its usefulness has been extended to include studies of rare-earth ions in glasses[2] and crystals.[3–6] The Eu^{3+} ion is the predominant choice as the rare-earth luminescent probe[5–9] because it is an almost ideal candidate for FLN. Excitation of the nondegenerate $^5D_0 \leftarrow {}^7F_0$ transition leads to fluorescence terminating on levels belonging to the ^7F_J ($J=0,1,\ldots,6$) multiplets. The multiplets are $2J+1$ degenerate and may be split into a maximum of $2J+1$ Stark components depending on the symmetry of the crystal field. Such transitions are parity forbidden in the free ion for electric dipole processes; however, in a crystal or glass, these transitions may become allowed as a consequence of coupling introduced by odd-parity terms in the crystal-field expansion.[10] The structure observed in the fluorescence spectrum (number of peaks) is then determined only by the splitting of the terminal levels caused by the local crystal field, because no Stark splitting of the emitting $^5D_0$ state can occur under any symmetry. Furthermore, the splitting of the terminal levels is very sensitive to local variations in the crystal field.

Most of the FLN literature has dealt only with site variations for ions in single-phase media (glasses or substitutionally doped crystals). It has been shown that FLN can be used to determine whether the Eu^{3+} ion is situated in a crystalline or glassy environment in partially crystallized phosphotungstate glasses.[11] Therefore, it would appear that the FLN technique can be a powerful tool to study phase separation and crystallization behavior in glasses, or glass ceramics.

The naturally occurring mineral sphene ($CaTiSiO_5$) is known to accept a wide variety of cationic impurities substitutionally at both the titanium and calcium sites.[12] Sphene-based glass ceramics (microcrystalline sphene within a continuous aluminosilicate glass matrix) are being investigated as a potential host matrix for the disposal of nuclear fuel recycle waste.[13] As such, it is of interest to determine how particular rare-earth ions substitute in such materials, which site or sites they occupy, and how they are partitioned between the sphene and glass phases of the glass ceramic. Synthetic sphene microcrystallites can be easily grown in a sodium aluminosilicate glass matrix by thermally induced crystallization of a glass of the appropriate composition.[13] The present work examines the Eu^{3+} emission from the sphene-based glass ceramic, the pure sodium aluminosilicate glass, and sphene ceramic (polycrystalline $CaTiSiO_5$).

The narrow spectral bandwidth of a dye laser has been used to excite only a small subset of Eu^{3+} ions out of the full ensemble of sites occupied in each of the glass, glass ceramic, and sphene ceramic. By tuning the laser frequency over the inhomogeneous bandwidth, different Eu^{3+} sites were sampled. From the excitation dependence of the peak positions of the Stark components of the $^7F_1$ and $^7F_2$ multiplets and by application of simple crystal-field theory a description of the local environment of the Eu^{3+} ion in the sphene ceramic and glass was obtained.

II. EXPERIMENTAL

The compositions of the sodium aluminosilicate glass, the glass ceramic (or phase-separated glass), and the sphene ceramic are given in Table I. Sodium has been in-

TABLE I. Composition of samples (wt. %).

Sample	CaO	Na_2O	Al_2O_3	TiO_2	SiO_2	Eu_2O_3
Aluminosilicate glass	3.90	11.15	14.18	1.76	68.0	1.07
Phase-separated glass or glass-ceramic	13.32	6.33	8.05	18.30	53.0	1.07
Sphene ceramic	28.6	0.18		40.38	30.37	1.07

troduced into the sphene ceramic to act as a charge compensator for Eu^{3+}, to allow it to be substitutionally incorporated into the sphene crystalline lattice ($Eu^{3+}+Na^{+}$ is expected to substitute for 2 Ca^{2+}).

The sodium aluminosilicate glass was prepared by melting the reagent-grade oxides and carbonates at 1500 °C in a platinum crucible, fritting by pouring into water, and crushing and remelting to ensure homogeneity. The melted glass was removed to a furnace at 800 °C and annealed for 1 h.

The sphene ceramic was prepared by melting the reagent-grade oxides at 1450 °C and fritting, then remelting and recrushing. The crushed frit was fully crystallized by heating to 1050 °C for 1 h and then wet milled under butanol for 24 h with alumina grinding media. The milled powder (0.2 to 2 μm) was blended with a binder (3 wt. % paraffin wax) and a plasticizer (1 wt. % stearic acid) in ether/carbon tetrachloride solution. After drying and granulating, 25-mm diameter pellets were pressed in a hardened steel die at 25 MPa. Sintering of the pellets was accomplished by heating them in air at 5 °C/min to 1310 °C and holding at this temperature for 3 h. X-ray diffraction results from a crushed pellet showed sphene to be the sole crystalline phase.

The glass ceramic was prepared by melting the reagent-grade oxides and carbonates at 1400 °C for 1 h followed by fritting, crushing, and remelting. The melt was then cast into a slab on a steel plate and annealed at 750 °C for 1 h. As demonstrated by Hayward and Cecchetto,[13] the glass phase separates on slow cooling from the melt into two amorphous phases: a CaO-, TiO_2-, SiO_2-rich droplet phase in a continuous Na_2O-, Al_2O_3-, SiO_2-rich phase. This phase-separated glass was subsequently reheated at 1050 °C for 2 h to induce crystallization of the sphene phase.

A Spectra Physics 375 Dye Laser operating with Rhodamine-6G (10^{-3} mol/dm^3 in ethylene glycol) pumped by a Spectra Physics 164 argon-ion laser was used for excitation of the FLN spectra. The laser had a typical linewidth of 2 cm^{-1} full width at half maximum (FWHM). Emission spectra with 514.5 nm excitation were excited directly with the green line of the argon-ion laser. The fluorescence was analyzed with a Ramanor U-1000, 1-m double monochromator (1800 groves/mm grating, first order, producing a dispersion 6.28 cm^{-1}/mm at 588 nm). Spectra were recorded using a maximum slit width of 300 μm, giving a minimum resolution of 2 cm^{-1}.

Samples were prepared for fluorescence by cleaning fractured or cut surfaces with acetone. Room-temperature emission spectra were recorded using the microscope attachment for the Ramanor U-1000. Low-temperature emission spectra were measured after mounting the sample in an Oxford Instruments CF204 continuous flow cryostat and cooling to 8 K.

III. RESULTS

Figure 1(a) shows the room temperature $^5D_0\rightarrow{}^7F_0,{}^7F_1,{}^7F_2$ region of the Eu^{3+} emission spectra excited at 514.5 nm from the sphene ceramic (top), the glass ceramic (middle), and the sodium aluminosilicate glass (bottom). We expect that the full ensemble of Eu^{3+} ions will be excited by the laser because light of this wavelength corresponds to an energy greater than that necessary to excite the $^5D_1\leftarrow{}^7F_0$ transition directly (peak at 522 nm). This is followed primarily by nonradiative relaxation from $^5D_1$ to $^5D_0$ and then emission to the ^7F_J multiplets.[9] (The room-temperature emission spectrum of Eu^{3+} in the phase-separated glass is identical to that from the sodium aluminosilicate glass. The low-temperature and FLN spectra from the phase-separated glass will not be considered here.) The corresponding spectra obtained at 8 K are shown in Fig. 1(b). Three salient features of these spectra are (1) that the full Stark splitting of the emissions to the $^7F_1$ (three components) and $^7F_2$ (five components) levels is observed, (2) the low-temperature sphene ceramic and glass-ceramic spectra are almost identical and show doublets with small splittings (20—40 cm^{-1}) for the $^7F_0$ and the two lowest components of the $^7F_1$ multiplet, indicating the existence of more than one coordination site, and (3) the sphene ceramic and the glass-ceramic spectra exhibit sharp emissions when compared with the sodium aluminosilicate glass spectrum.

The broad inhomogeneous line profile for the $^5D_0\rightarrow{}^7F_0$ transition in the sodium aluminosilicate glass at 8 K (574.0—581.0 nm, 123 cm^{-1} FWHM) arises from the large site-to-site variations of the crystal-field strength. For the $^5D_0\rightarrow{}^7F_1$ transition, three broad overlapping lines are observed (581—604 nm) corresponding to emission to the three Stark components of the $^7F_1$ state. The linewidth of each component is about 170 cm^{-1}. For the $^5D_0\rightarrow{}^7F_2$ transition, a broad incompletely resolved band containing the five Stark components is seen (604—635 nm). The full width is about 730 cm^{-1}.

For the sphene ceramic spectra, the three- and five-line multiplets for the $^5D_0\rightarrow{}^7F_1$ (578—600 nm) and $^5D_0\rightarrow{}^7F_2$ (607—629 nm) transitions are fully resolved. However, the linewidths of each component of the doubled $^5D_0\rightarrow{}^7F_0$ transition in the sphene ceramic at 8 K

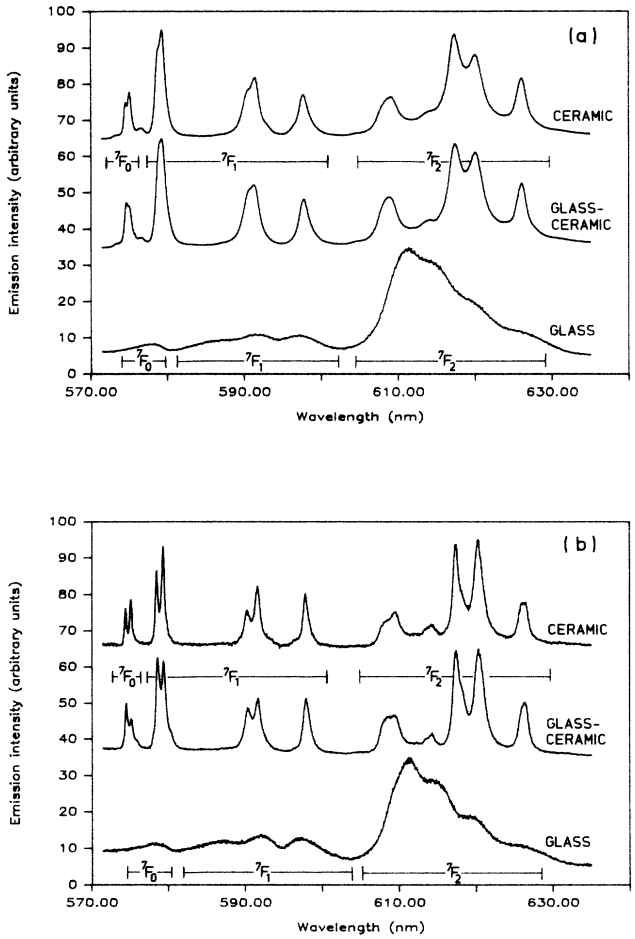

FIG. 1. Emission spectra of Eu^{3+} in sphene ceramic (top), glass ceramic (center), and sodium aluminosilicate glass (bottom). Excited at 514.5 nm and observed at (a) room temperature and (b) 8 K.

(574.0—576.0 nm, 12 cm^{-1} FWHM) are still broad compared with the homogeneous linewidths of Eu^{3+} in a single crystal such as Gd_2O_3:Eu^{3+} (2 cm^{-1}).[14]

Figures 2 and 3 show the 8 K emission spectra of the aluminosilicate glass and sphene ceramic, respectively, excited at various wavelengths within the $^5D_0 \rightarrow {}^7F_0$ emission bands (which should correspond closely to the respective absorption bands due to the small Stoke's shift usually observed in rare-earth ions). The most important features are the sharpness of the lines when compared with the spectra excited at 514.5 nm (FLN) and the excitation dependent shift of the lowest component of the $^5D_0 \rightarrow {}^7F_1$ transition.

In addition to the full Stark splitting observed in the sphene ceramic FLN spectra, further splittings are observed, indicating the excitation of more than one site. For example, in the 574.4-nm spectrum, the three $^7F_1$ components are assigned to the peaks appearing 121, 459, 688 cm^{-1} below the excitation wavelength. Along with these are weaker satellite peaks at 113, 507, and 651 cm^{-1}. No satellite peaks are seen in the $^7F_2$ region, but some of the peaks show a broadening to one side, indicating the underlying presence of another peak. For the sub-

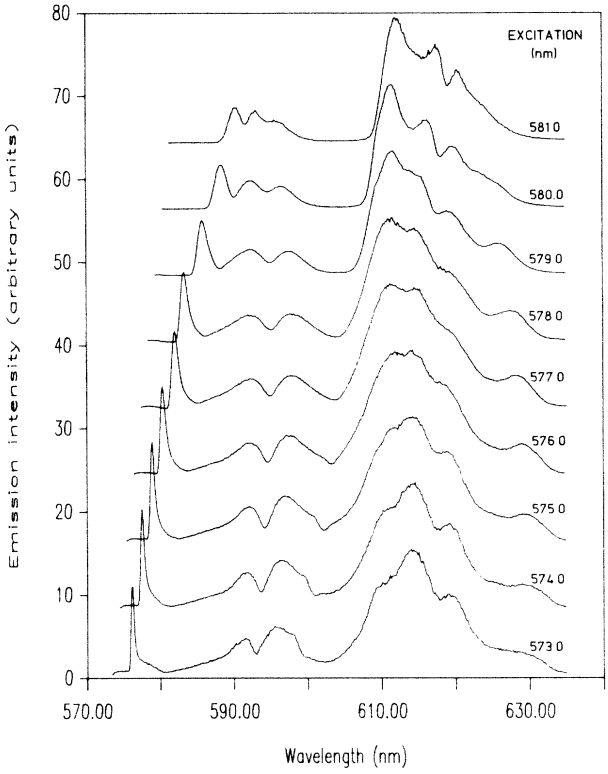

FIG. 2. Emission spectra of Eu^{3+} in sodium aluminosilicate glass at 8 K using different excitation wavelengths.

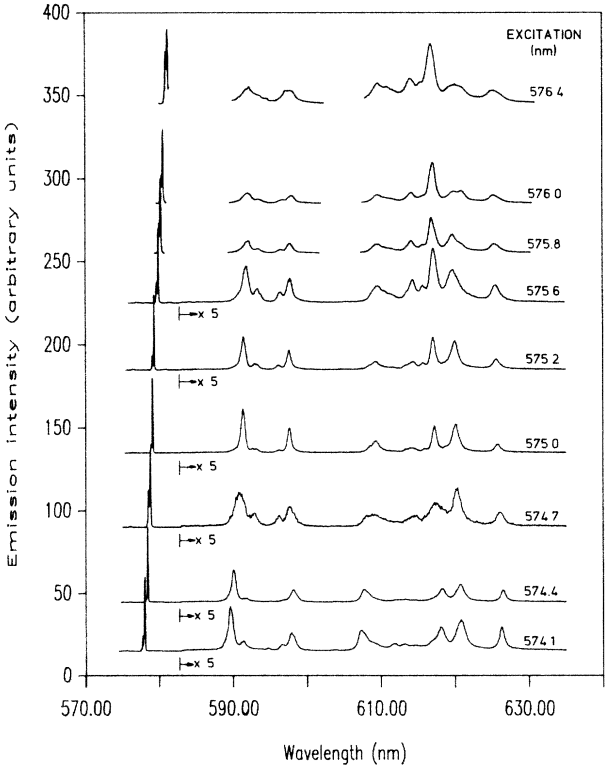

FIG. 3. Emission of spectra of Eu^{3+} in the sphene ceramic at 8 K using different excitation wavelengths. Spectra are scaled to largest peak. The vertical displacement of each spectrum is proportional to the change in excitation wavelength.

sequent discussion, only the strongest peaks will be considered and these satellite peaks will be ignored. A full treatment of this complication has not yet been completed, but work is under way to identify the extra components by fitting the spectra.

The energies of the $^7F_0$ ground state and the Stark components of the $^7F_1$ and $^7F_2$ multiplets with respect to $^5D_0$ at each excitation are plotted in Figs. 4 and 5 as a function of the pump wavelength ($^5D_0$ excitation energy) for the glass and sphene ceramic, respectively.

IV. DISCUSSION

The line-narrowing effect is immediately evident in all the low-temperature spectra excited by the dye laser. If we consider the range of wavelengths used for excitation in the glass (573.0–581.0 nm) and the sphene ceramic (574.2–576.4 nm), they span the width of the $^5D_0 \rightarrow {}^7F_0$ emission band in the respective 8-K spectra excited at 514.5 nm. Considering the wavelengths of the lowest component of the $^5D_0 \rightarrow {}^7F_1$ multiplet, we find that the range of the peak positions in the line-narrowed spectra (576.4–590.4 nm for the glass and 578.2–583.1 nm for the sphene ceramic) spans the width of the corresponding emission band in the respective 8-K spectrum excited at 514.5 nm. Furthermore, the wavelengths of the other components of the $^5D_0 \rightarrow {}^7F_1$ transition and all components of the $^5D_0 \rightarrow {}^7F_2$ transition vary only slightly (1 or 2 nm) and correspond to the wavelengths of the respective emission excited at 514.5 nm.

The excitation range and range of energies of the components of the $^7F_1$ and $^7F_2$ emissions are given in Table II for the glass and sphene ceramic. For comparative purposes, the corresponding values for Eu^{3+} emission for sodium-barium-zinc silicate,[7] potassium fluoroberyllate,[8] lithium borate,[9] sodium phosphotungstate,[11] and calcium phosphate[15] glasses and europium phosphate,[16] lanthanum fluoride,[17] lanthanum-magnesium borate,[18] and yttrium-aluminum garnet[6] crystals are also included. The ranges of values for all systems are comparable; however, the largest overlap is between the aluminosilicate glass and the sodium-barium-zinc silicate glass, which is not unexpected since both are silicate-based systems.

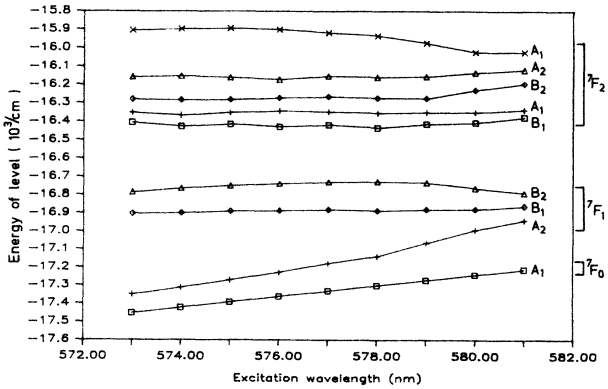

FIG. 4. Energy of the Stark components of the $^7F_0$, $^7F_1$, and $^7F_2$ emissions of Eu^{3+} in sodium aluminosilicate glass relative to the $^5D_0$ emitting level at each excitation as a function of excitation wavelength.

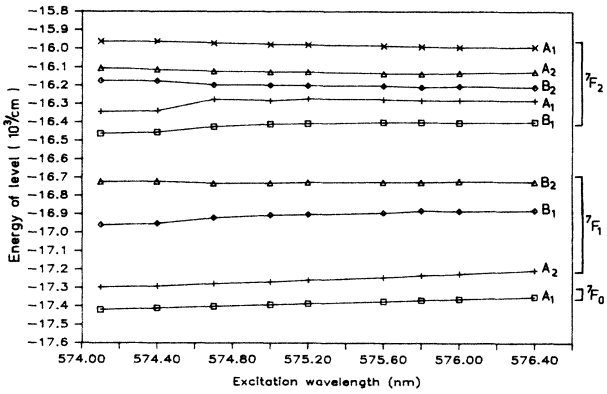

FIG. 5. Energy of the Stark components of the $^7F_0$, $^7F_1$, and $^7F_2$ emissions of Eu^{3+} in calcium titanosilicate sphene relative to the $^5D_0$ emitting level at each excitation as a function of excitation wavelength.

The crystal-field Hamiltonian ($\mathscr{H}_c$) is most conveniently written in the operator equivalent form[19]

$$\mathscr{H}_c = \sum_n \sum_m \theta_j^n (B_{nm}^c O_{nm}^c + B_{nm}^s O_{nm}^s) , \tag{1}$$

where

$$B_{nm}^{c,s} = A_{nm}^{c,s} \langle r^n \rangle = - |e| K_n \langle r^n \rangle \gamma_{nm}^{c,s} \tag{2}$$

are the crystal-field parameters; $O_{nm}^{c,s}$ are the operator equivalent expressions; θ_j^n is the operator equivalent factor α_j, β_j, or γ_j; K_n is a normalizing factor; and $\gamma_{nm}^{c,s}$ are the lattice sums. The various entries in the secular determinant are

$$\langle JM | \mathscr{H}_c | JM' \rangle = H_{MM'} \tag{3}$$

and are easily evaluated from the published tables.[20]

Although the true site symmetry of Eu^{3+} is C_1 in both the glass (no long-range order) and the sphene [space group $P2_1/a$ (C_{2h}^5) with four molecules per unit cell[21]], the crystal-field calculations are based on the assumption of C_{2v} point-group symmetry. This symmetry is the highest noncentrosymmetric symmetry for which the full Stark splitting of the J manifolds occurs (highest symmetry with no degenerate representations) and the lowest symmetry for which symmetry distinctions of most of the components are maintained. Emission from Eu^{3+} is more sensitive to its first coordination shell than to its more distant neighbors, and it is expected that this shell will have higher than C_1 symmetry.[7,16] In fact, the coordinating oxygen polyhedron of Ca^{2+}, for which Eu^{3+} is expected to substitute in the sphene,[22] approximates C_{2v} symmetry.[23] Lempicki *et al.*[19] give the details for performing the crystal-field calculations. Using their equations for C_{2v} symmetry, a set of crystal-field parameters, B_{nm}, giving the best fit to all eight components was derived for each spectrum. The best fit was determined by using a simplex algorithm to minimize the sum of squared residuals between the observed and calculated peak positions. The fits for spectra obtained from the glass using the symmetry assignments of Brecher and Riseberg[7] were

TABLE II. Excitation range and range of energy levels (cm^{-1}) for Eu^{3+}-doped glasses and crystals.

Sample[a]	Excitation range (nm)	$^7F_1$			$^7F_2$				
		Glasses							
$Na_2O{\cdot}Al_2O_3{\cdot}SiO_2$	573.0–581.0	102–274	550–350	666–422	1045–833	1099–875	1171–1016	1294–1093	1547–1188
$Na_2O{\cdot}BaO{\cdot}ZnO{\cdot}SiO_2$ [b]	573.0–581.0	103–294	560–334	679–430	1037–821	1085–853	1169–1002	1315–1080	1457–1196
$KF{\cdot}CaF_2{\cdot}AlF_3{\cdot}BeF_2$ [c]	575.6–578.7	110–340	233–395	635–455	785–946	886–1023	1111–1065	1212–1175	1255–1216
$LiO_2{\cdot}B_2O_3$ [d]	575.0–581.0	131–279	439–356	668–453					
$Na_2O{\cdot}P_2O_5{\cdot}WO_3$ [e]	577.5–580.0	200–312	444–375	612–452					
$Ca(PO_3)_2$ [f]	577.6–580.0	198–294	432–368	568–440					
		Crystals							
$CaTiSiO_5$	574.1–576.4	123–146	459–469	695–625	957–949	1077–1067	1245–1140	1315–1225	1457–1357
EuP_5O_{14} [g]	578.4	271	392	474	937	960	1070	1097	1180
LaF_3 [h]	578.3	313	375	415		964	997	1098	
$LaMgB_5O_{10}$ [i]	577.6	243	338	635	909	937	1149	1182	1250
$Y_3Al_5O_{12}$ [j] I	577.3	286	372	400	879	914	1022	1314	1432
$Y_3Al_5O_{12}$ [j] II	580.9	281	305	455	709	820	1167	1186	1241

[a]The sample identifications give only the chemical components of the glass and not their molar ratios.
[b]Reference 7.
[c]Reference 8.
[d]Reference 9.
[e]Reference 11.
[f]Reference 15.
[g]Reference 16.
[h]Reference 17.
[i]Reference 18.
[j]Reference 6.

very good with a root-mean-squared (rms) deviation between the fitted and observed peak positions of < 10 cm^{-1} (Table III). The rms deviation using the same assignments for the sphene ceramic was ~ 30 cm^{-1} (Table IV). However, the residuals obtained when the assignment proposed by Brecher[16] for EuP_5O_{14} is used are even higher. The calculations were repeated for the sphene ceramic using all 340 possibilities with the lowest component of the $^7F_1$ multiplet assigned a symmetry of A_1. There are 12 distinct assignments with lower residuals than the one used here, but there is no physical basis for choosing one over another. Work is currently under way to see if any of these assignments would be a better choice. The crystal-field parameters obtained are listed in Tables V and VI for the sodium aluminosilicate glass and the sphene ceramic, respectively.

TABLE III. Eu^{3+} energy levels (cm^{-1}) in sodium aluminosilicate glass as a function of pump wavelength assuming C_{2v} symmetry.

Excitation (nm)	Symmetry assignment								
	$^7F_1$			$^7F_2$					
	A_2	B_1	B_2	B_1	A_1	B_2	A_2	A_1	rms dev.
573.0 obs	102	550	666	1045	1099	1171	1294	1547	
calc	110	550	658	1045	1092	1165	1301	1554	6.3
574.0 obs	110	522	658	994	1053	1136	1269	1524	
calc	109	522	659	994	1054	1137	1268	1523	0.6
575.0 obs	122	502	642	975	1039	1109	1231	1497	
calc	120	502	644	975	1041	1111	1230	1495	1.6
576.0 obs	134	474	622	931	1017	1088	1189	1460	
calc	133	474	623	931	1018	1089	1188	1459	0.7
577.0 obs	154	450	602	911	982	1064	1178	1413	
calc	149	448	610	909	988	1070	1174	1407	5.3
578.0 obs	162	414	574	865	945	1027	1142	1367	
calc	156	410	584	861	953	1035	1137	1359	7.1
579.0 obs	206	390	538	855	919	995	1116	1297	
calc	199	381	554	848	932	1008	1111	1284	10.9
580.0 obs	250	362	478	834	890	1012	1108	1218	
calc	249	353	488	827	899	1020	1107	1209	7.4
581.0 obs	274	350	422	833	875	1016	1093	1188	
calc	276	335	435	821	888	1026	1095	1175	11.2

TABLE IV. Eu^{3+} energy levels (cm^{-1}) in calcium titanosilicate sphene as a function of pump wavelength assuming C_{2v} symmetry.

Excitation (nm)	Symmetry assignment $^7F_1$ A_2	B_1	B_2	$^7F_2$ B_1	A_1	B_2	A_2	A_1	rms dev.
574.1 obs	123	459	695	957	1077	1245	1315	1457	
calc	150	480	647	974	1038	1206	1337	1496	33.1
574.4 obs	120	459	688	955	1073	1235	1299	1449	
calc	148	478	641	971	1034	1196	1322	1488	32.8
574.7 obs	125	480	668	976	1126	1204	1280	1430	
calc	158	495	620	988	1086	1165	1307	1470	34.0
575.0 obs	125	485	661	981	1109	1193	1267	1413	
calc	157	497	616	991	1071	1156	1294	1451	32.1
575.2 obs	129	483	659	977	1113	1185	1261	1405	
calc	162	496	613	987	1074	1148	1288	1444	32.7
575.6 obs	132	480	648	972	1098	1172	1240	1388	
calc	164	491	604	981	1061	1136	1267	1425	31.4
575.8 obs	136	485	641	965	1086	1158	1232	1377	
calc	166	495	602	973	1052	1126	1256	1411	28.4
576.0 obs	138	476	640	957	1080	1157	1230	1368	
calc	168	487	599	966	1046	1124	1254	1402	29.2
576.4 obs	146	469	625	949	1067	1140	1225	1357	
calc	170	479	591	957	1039	1112	1244	1385	24.0

TABLE V. Crystal-field parameters (cm^{-1}) assuming C_{2v} symmetry for Eu^{3+} in sodium aluminosilicate glass.

Excitation (nm)	E_1	B_{20}	B_{22}	E_2	B_{40}	B_{42}	B_{44}
573.0	439.3	−823.3	271.4	1231.2	−79.2	696.0	−891.5
574.0	430.0	−801.9	342.3	1195.2	−90.3	844.6	−837.4
575.0	422.0	−754.5	355.8	1170.2	−95.3	828.6	−873.3
576.0	410.0	−691.8	372.8	1137.0	−107.7	929.4	−844.4
577.0	402.0	−632.9	404.7	1109.6	−105.7	968.3	−644.7
578.0	383.3	−567.7	436.6	1069.2	−120.9	1045.3	−521.0
579.0	378.0	−446.0	431.9	1036.4	−122.2	987.3	−272.3
580.0	363.0	−285.5	336.0	1012.4	−116.4	1037.4	159.7
581.0	348.7	−181.4	249.8	1001.0	−115.0	1016.0	324.3

TABLE VI. Crystal-field parameters (cm^{-1}) assuming C_{2v} symmetry for Eu^{3+} in sphene.

Excitation (nm)	E_1	B_{20}	B_{22}	E_2	B_{40}	B_{42}	B_{44}
574.1	425.7	−689.3	419.3	1210.2	−94.6	1259.6	−232.9
574.4	422.3	−686.4	406.6	1202.2	−91.8	1223.9	−282.7
574.7	424.3	−666.0	312.2	1203.2	−112.1	952.2	−393.8
575.0	423.7	−665.1	297.8	1192.6	−97.0	897.0	−398.2
575.2	423.7	−654.0	294.1	1188.2	−102.8	873.8	−395.4
575.6	420.0	−638.9	283.0	1174.0	−95.1	844.4	−420.5
575.8	420.7	−637.2	267.9	1163.6	−93.6	823.9	−414.5
576.0	418.0	−626.2	279.8	1158.4	−94.2	850.4	−373.8
576.4	413.3	−609.0	280.2	1147.6	−96.3	841.9	−338.7

Brecher and Riseberg previously analyzed possible coordination structures for sodium-barium-zinc silicate glasses.[7] They found that the full range of experimental crystal-field parameters could be adequately explained by eight equidistant coordinating oxygens arranged in a somewhat disordered Archimedean antiprism (symmetry C_{2v}) into which a ninth coordinating oxygen gradually intrudes along the axial direction. Based on the similarity of the range of values for the sodium aluminosilicate glass and the sodium-barium-zinc silicate glass (Table II), it appears appropriate to apply their model for this study.

Pure orientational information about the coordination can be extracted by considering the ratios of crystal-field parameters of the same order (B_{22}/B_{20} and B_{44}/B_{40}).[7] The ratios B_{44}/B_{40} are plotted against $-B_{22}/B_{20}$ in Fig. 6 for the glass and the sphene ceramic. Brecher and Riseberg's ratios, calculated from the geometric model ranging from pure eightfold coordination to pure ninefold coordination, are also included. The sodium aluminosilicate glass values follow the theoretical ones quite well, indicating the presence of sites covering the full range of 8 to 9 coordination. On the other hand, the values for the crystalline sphene do not fall on the theoretical line, confirming that the coordination of Eu^{3+} in the sphene is not the same as in the glass. This is consistent with Eu^{3+} substituting for Ca^{2+} in a sevenfold coordination site. The clustering of the points in two groups though indicates that at least two distinct Eu^{3+} sites exist and that the geometrical environment of the Eu^{3+} ion in each of them is constant. One site has an excitation range of 574.2 to 574.5 nm, while the other has an excitation range of 574.5 to 576.4 nm. This can be seen in Fig. 5 as the discontinuity in the energy of some of the Stark components between 574.4 and 574.6 nm. A multiplicity of sites would result from the various possible charge compensation arrangements. One way in which two distinct sites would arise is from having the closest Ca^{2+} site being occupied by either Ca^{2+} (with remote charge compensation) or Na^{+} (local charge compensation). Then the additional splittings mentioned earlier could arise from different remote sites occupied by Na^{+} charge compensators (for example, next nearest Ca^{2+}).

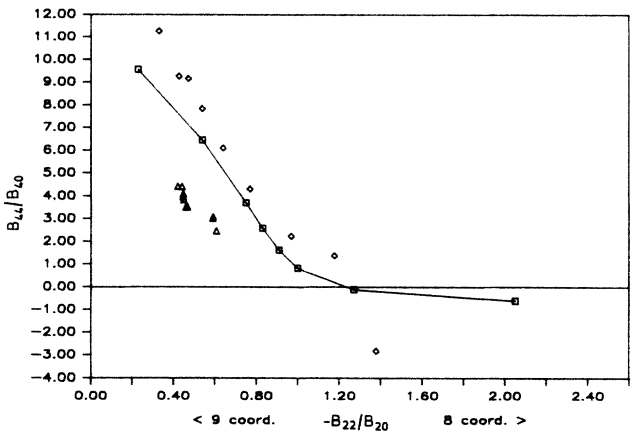

FIG. 6. Behavior of the major crystal-field ratios B_{22}/B_{20} and B_{44}/B_{40} which contain purely geometric information about the coordination. The line and □ symbols represent values calculated from the geometric model [Brecher and Riseberg (Ref. 7)]. The ◇ symbols indicate experimental values for sodium aluminosilicate glass and the △ symbols represent values for the sphene ceramic.

One of the goals of this study was to determine the partitioning ratio for Eu^{3+} between sphene and glass phases of the glass ceramic. If we return to consider Fig. 1, no glass-type emission is seen in the glass-ceramic spectrum (middle). Even after computer subtraction of the sphene ceramic spectrum (top) from the glass-ceramic spectrum, no glass-type spectrum was observed. FLN spectra for the glass ceramic excited at different wavelengths between 574.5 and 580.0 nm are shown in Fig. 7. At excitations between 574.5 and 576.5 nm (bottom four spectra), pure sphene-type spectra are seen. At excitations between 578.0 and 580.0 nm (top three spectra) pure glass-type spectra are observed. The splittings in each spectrum correspond to the splittings observed in the respective single-phase sphene or glass spectrum recorded at the same excitation wavelength. The fifth spectrum from the bottom, excited at 577.0 nm, shows a mixture of sphene- and glass-type spectra.

In an attempt to estimate the partitioning ratio for Eu^{3+}, spectra of the $^5D_0 \rightarrow {}^7F_1$ emission range were recorded using excitations between 573.5 and 580.0 nm at 0.5-nm intervals, keeping the exciting laser power constant at 50 mW. The total integrated peak area for the $^7F_1$ emissions are given for each spectrum in Table VII.

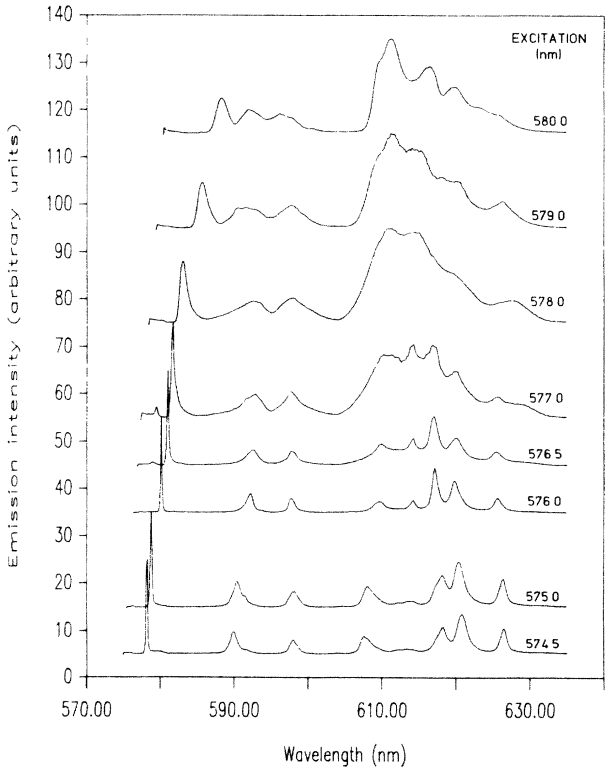

FIG. 7. Emission spectra of Eu^{3+} in the glass ceramic at 8 K as a function of excitation wavelength. Spectra are scaled to largest peak. The vertical displacement of each spectrum is proportional to the change in excitation wavelength.

TABLE VII. Integrated areas of glass-ceramic $^7F_1$ emission multiplet at constant laser power of 50 mW.

Excitation (nm)	Peak area	Use for average
573.5	79 200	
574.0	4620 000	sphene
574.5	4080 000	sphene
575.0	2860 000	sphene
575.5	1120 000	sphene
576.0	816 000	sphene
576.5	215 000	
577.0	173 000	
577.5	163 000	glass
578.0	186 000	glass
578.5	186 000	glass
579.0	147 000	glass
579.5	141 000	glass
580.0	6880	

The data clearly show that the excitation peaks for both the sphene and glass phases were sampled. The average integrated area for the sphene phase (574.0—575.5 nm) is $(3.2\pm1.3)\times10^6$ while that for the glass phase (577.5—579.5 nm) is $(1.65\pm0.19)\times10^5$. The total Eu^{3+} emission intensity can be calculated by dividing the integrated areas of the $^7F_1$ emissions by the fraction of the total emission that is $^7F_1$. From Fig. 1(b), the $^7F_0$ emission is 5 and 2% of $^7F_0+^7F_1+^7F_2$ in the sphene and glass, respectively. The total of $^7F_3+^7F_4+^7F_5+^7F_6$ is expected to be even less because of the selection rules. Therefore the $^7F_0$ and $^7F_3$ through $^7F_6$ emissions can be neglected in the total emission intensity with the introduction of only a 5% error. From Figs. 2 and 3, the ratio $^7F_1/(^7F_1+^7F_2)$ is constant in each spectrum and equal to 0.51 ± 0.02 in the sphene and 0.22 ± 0.02 in the glass.

Electron microscopy of the glass ceramic[24] showed that the sphene crystallites were elongated crystals ~1 μm in diameter and 10 to 20 μm in length occupying 40—50% of the specimen volume. If we assume that the effective interrogated volumes of the sphene and glass phases are equal (this may not be exactly true due to topological considerations and different penetration for the exciting laser in the two phases), then the ratio of the estimated total emission should give the Eu^{3+} partition ratio. With the above assumptions, the partition ratio is 8:1 sphene phase/glass phase. It must also be noted that an implicit assumption in this calculation is that the absorption coefficient is equal for Eu^{3+} in both phases. This is not an unreasonable assumption because the $^5D_0\leftarrow^7F_0$ transition is not known to be hypersensitive.[25] The ratio calculated here is of the same order of magnitude as that determined for La ($\sim$2:1) and Ce (2 to 6:1) by transmission electron microscopy coupled with energy-dispersive x-ray analysis.[26]

Now it can be understood why no glass-type emission can be seen in the glass-ceramic spectrum excited at 514.5 nm. Although only ~8 times as much Eu^{3+} is in the sphene phases as in the glass phase, the peaks in the glass phase are ~5—10 times as broad as those in the sphene phase. This makes the peak intensity of the Eu^{3+} emission from the glass phase 40—80 times smaller than that from the sphene phase.

V. CONCLUSIONS

In the foregoing discussion, it was shown that the structural model Brecher and Riseberg[7] developed for sodium-barium-zinc silicate glasses gives acceptable agreement when applied to the sodium aluminosilicate glass system. The sites occupied by Eu^{3+} in the sphene ceramic (at least two different sites) do not fit this coordination scheme, but the coordination around Eu^{3+} appears constant in each site. By selective excitation of Eu^{3+}, it was shown that the ion substitutes in both the sphene and glass phases of the glass ceramic, with a partitioning ratio estimated to be 8:1 (sphene phase/glass phase).

ACKNOWLEDGMENTS

The authors wish to thank Dr. C. Brecher of the GTE Laboratories, Inc., Waltham, MA, and E. R. Vance of AECL, Pinawa, Manitoba for their helpful discussions. This research was supported by Atomic Energy of Canada, Ltd. (AECL), Whiteshell Nuclear Research Establishment, Pinwawa, Manitoba. We also gratefully acknowledge the Natural Sciences and Engineering Research Council of Canada and the Faculty of Graduate Studies and Research, McGill University for financial support.

*Present address: Department of Chemistry, Concordia University, Montreal, Quebec, Canada H3G 1M8.

[1]A. Szabo, Phys. Rev. Lett. **25**, 924 (1970); **27**, 323 (1971).

[2]L. A. Riseberg, Phys. Rev. Lett. **28**, 786 (1972); C. Brecher, L. A. Riseberg, and M. J. Weber, Phys. Rev. B **18**, 5799 (1978); M. J. Weber, J. A. Paisner, S. S. Sussman, W. M. Yen, L. A. Riseberg, and C. Brecher, J. Lumin. **12/13**, 729 (1976); A. F. Leung, J. Non-Cryst. Solids **21**, 41 (1976).

[3]J. B. Gruger, unpublished results, quoted by C. A. Morrison and R. P. Leavitt, in *Handbook on the Physics and Chemistry of Rare Earths,* edited by K. A. Gschneidner and L. R. Eyring (North-Holland, Amsterdam, 1982), Vol. 5, p. 578.

[4]R. J. Danby and N. B. Manson, J. Chem. Phys. **81**, 5462 (1984).

[5]J. Dexpert-Ghys, M. Faucher, and P. Caro, Phys. Rev. B **23**, 607 (1981); S.-I. Mho and J. C. Wright, J. Chem. Phys. **77**, 1183 (1982); J. R. Wietfeldt and J. C. Wright, J. Lumin. **31/32**, 263 (1984); J. Dexpert-Ghys, M. Faucher, and P. Caro, J. Solid State Commun. **41**, 27 (1982).

[6]M. Asano and J. A. Koningstein, Chem. Phys. **42**, 369 (1981).

[7]C. Brecher and L. A. Riseberg, Phys. Rev. B **13**, 81 (1976).

[8]C. Brecher and L. A. Riseberg, Phys. Rev. B **21**, 2607 (1980).

[9]J. Hegarty, W. M. Yen, and M. J. Weber, Phys. Rev. B **18**, 5816 (1978).

[10]B. R. Judd, Phys. Rev. **127**, 750 (1962); G. S. Ofelt, J. Chem. Phys. **37**, 511 (1962).

[11]H. Mack, G. Boulon, and R. Reisfeld, J. Lumin. **24/25**, 111 (1981); F. Durville, G. Boulon, R. Reisfeld, H. Mack, and C. K. Jorgensen, Chem. Phys. Lett. **102**, 393 (1983).

[12]I. I. Zabavnikova, Geochem., 271 (1957); M. H. Staatz, N. M. Conklin, and I. K. Brownfield, J. Res. U.S. Geol. Surv. **5**, 623 (1977).

[13]P. J. Hayward and E. V. Cecchetto, *Scientific Basis for Nuclear Waste Management,* Vol. 6. of *Materials Research Society Symposia Proceedings,* edited by S. V. Topp (American Elsevier, New York, 1982), p. 91.

[14]D. K. Rice and L. G. DeShazer, Phys. Rev. **186**, 387 (1969).

[15]N. Motegi and S. Shionoya, J. Lumin. **8**, 1 (1973).

[16]C. Brecher, J. Chem. Phys. **61**, 2297 (1974).

[17]U. V. Kumar, D. R. Rao, and P. Venkateswarlu, J. Chem. Phys. **66**, 2019 (1977).

[18]J. Holsa and M. Leskela, Mol. Phys. **54**, 657 (1985).

[19]A. Lempicki, H. Samelson, and C. Brecher, J. Mol. Spectrosc. **27**, 375 (1968).

[20]M. T. Hutchings, Solid State Phys. **16**, 227 (1964).

[21]J. A. Speer and G. V. Gibbs, Am. Mineral. **61**, 238 (1976).

[22]J. B. Higgins and P. H. Ribbe, Am. Mineral. **61**, 878 (1976); P. H. Ribbe, in *Review in Mineralogy,* edited by P. H. Ribbe (Mineralogical Society of America, Washington, 1980), Vol. 5, p. 143.

[23]From atomic positions in Ref. 21. A diagram of the Ca^{2+} coordination shell in the previously reported $C2/c$ space group for sphene is given in W. L. Bragg, *Atomic Structure of Minerals* (Cornell University Press, Ithaca, New York, 1937), p. 160.

[24]W. H. Hocking (private communication).

[25]R. D. Peacock, Struct. Bonding (Berlin) **22**, 83 (1975).

[26]P. J. Hayward, E. R. Vance, C. D. Carr, and S. L. Mitchell, in *Advances in Ceramics,* edited by G. G. Wicks, and W. A. Ross (American Ceramic Society, Columbus, Ohio, 1984), Vol. 8, p. 291.